Nonlinear Analysis: Modelling and Control, Online First, 1–16
https://doi.org/10.15388/namc.2024.29.35395

Vilnius University Press

Hysteresis and bistability in synaptic transmission modeled as a chain of biochemical reactions with a positive feedback

Pranas Katauskis[a], **Feliksas Ivanauskas**[a], **Aidas Alaburda**[b]

[a]Faculty of Mathematics and Informatics, Vilnius University,
Naugarduko str. 24, LT-03225 Vilnius, Lithuania
pranas.katauskis@mif.vu.lt; feliksas.ivanauskas@mif.vu.lt;

[b]Institute of Biosciences, Life Sciences Center, Vilnius University,
Saulėtekio ave. 7, LT-10257 Vilnius, Lithuania
aidas.alaburda@gf.vu.lt

Received: January 30, 2024 / **Revised:** May 9, 2024 / **Published online:** June 25, 2024

Abstract. In this paper, we employ computational analysis to investigate the long-term potentiation (LTP) and memory formation in synapses between neurons. We use a mathematical model describing the synaptic transmission as a signal transduction pathway with a positive feedback loop formed by diffusion of nitric oxide (NO) to the presynaptic site. We found that the model of synaptic transmission exhibits a hysteresis-like behavior, where the strength of synaptic transmission depends not just on instantaneous interstimulus intervals, but also on the history of activity. The switching between resting and memory states can be induced by physiologically relevant and moderate (less than 50%) changes in the duration of interstimulus intervals.

Keywords: long-term potentiation, memory, modeling, positive feedback loop, bistability, hysteresis-like behavior, information processing.

1 Introduction

Memory, learning, and adaptation to a changing environment in animals, examples of multistable behavior, are essential features to survival. The storage of information in the brain is associated with altered synaptic connectivity between neurons. The long-term potentiation (LTP) – a long-lasting increase in synaptic strength induced by short-term stimuli – is used for experimental studies of learning and memory [7].

A number of post- and presynaptic mechanisms are involved in LTP, including modification of proteins, intracellular Ca^{2+} signaling, diffusion of NO, altered gene expression, and insertion and internalization of receptors [2,3]. Also, mechanisms of LTP are specific to types of neurons and region of the brain.

The loss of memory and impaired ability of new memory formation are the hallmarks of Alzheimer's desease (AD) [15]. The experiments in animal models demonstrated that

Amyloid beta, associated with memory loss in AD, can cause an impairment of LTP [27]. Moreover, Amyloid beta inhibits a NO-dependent pathway during LTP [24]. A number of other neurological and neurodegenerative deseases are associated with impaired memory.

Understanding neuronal mechanisms behind LTP is critical for understanding memory, learning, and impairments during neurodegenerative diseases. Despite the recent advancement in neuroscience, we are still limited by the experimental design and techniques for exploring the mechanisms and pathways involved in LTP [9]. This increases the need for theoretical and modeling studies revealing and explaining the possible mechanisms of LTP.

From a theoretical perspective memory, learning and adaptation to a changing environment can be considered as examples of multistable behavior. Systems with positive feedback under certain conditions may exhibit multistable behavior [17] when a short-lasting stimulus or perturbation in the environment can lead to a long-lasting change in the system behavior [14, 20].

In the previous paper [11], we demonstrated that the long-term potentiation of synaptic transmission can be explained as a bistable behavior in a chain of biochemical reactions with positive feedback (Fig. 1). In that case the dynamics of glutamate (Glu), calcium (Ca^{2+}), and nitric oxide (NO) (Fig. 1a), forming the positive feedback loop by diffusing to the presynaptic site and facilitating the release of Glu (Fig. 1b), were described by a system of nonlinear diffusion–reaction equations with Michaelis–Menten (MM) kinetics.

One of the feature of model proposed in [10, 11] was that the test stimuli every 5 s were required not only to test the synaptic strength, but to maintain the elevated NO concentration as well. Can this model be applicable under real conditions? Even at rest in a brain, there is some spontaneous synaptic activity [22], which may keep elevated concentrations of NO under real conditions. Moreover, the increased brain activity is associated with decrease of time intervals between action potentials, whereas the decreased brain activity with increased time intervals between action potentials. The physiological activity and coding of information in a brain is associated with changes of time interval between action potentials.

In this study, we investigated the behavior of proposed LTP model with physiologically relevant interstimulus intervals. Here we demonstrate that interstimulus intervals comparable to background brain activity are sufficient to maintain the memory state. Memorizing and forgetting can occur even by a moderate (less than 50%) change in interstimulus intervals. Moreover, the LTP model proposed exhibits a hysteresis-like behavior in response to changes in the interstimulus intervals.

2 Model description

In this investigation, we used the previously proposed LTP model [10, 11]. The synapse is described as a one-dimensional object consisting of a presynaptic terminal, synaptic cleft, and postsynaptic terminal (Fig. 1(a)).

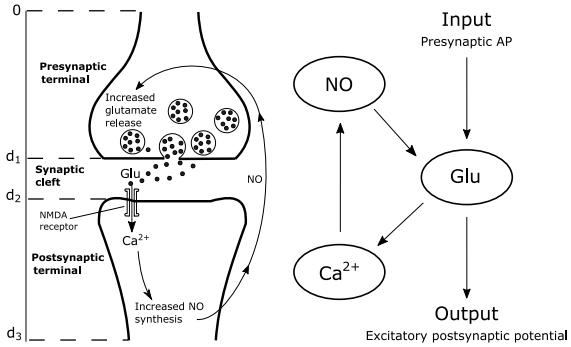

Figure 1. Graphical representation of the proposed LTP model. (a) The detailed schematic diagram of glutamate (Glu), calcium (Ca^{2+}), and nitric oxide (NO) forming a signal transduction pathway of LTP with positive feedback. (b) The schematic view of positive feedback loop of LTP model.

The concentrations of nitric oxide ($[NO](t,x)$), glutamate ($[Glu](t,x)$), and calcium Ca^{2+} ($[Ca](t,x)$) are functions of two variables, the time t and the position x. Interactions between substances are modeled as one-to-one chemical reactions between substrate and enzyme. Coupled systems of partial differential equations for $[NO]$, $[Glu]$, and $[Ca]$ are considered.

The differential equation for $[NO]$ is investigated in the domain $[0,d_3]$, the differential equation for $[Glu]$ is stated in the domain $[d_1,d_2]$, and the Ca^{2+}-concentration is considered in $[d_2,d_3]$.

The NO dynamics and NO producing in Ca^{2+}-dependent manner at the postsynaptic terminal are described by the reaction–diffusion equations

$$\begin{aligned}
\frac{\partial[NO]}{\partial t} &= D_{\mathrm{NO}}\frac{\partial^2[NO]}{\partial x^2} - \left(k_1 + \frac{v_{\max}^{\mathrm{NO}}}{k_M^{\mathrm{NO}} + [NO]}\right)[NO] \quad \text{for } 0 < x < d_2,\ t > 0,\\
\frac{\partial[NO]}{\partial t} &= D_{\mathrm{NO}}\frac{\partial^2[NO]}{\partial x^2} - \left(k_1 + \frac{v_{\max}^{\mathrm{NO}}}{k_M^{\mathrm{NO}} + [NO]}\right)[NO]\\
&\quad + k_2\big([Ca] - Ca^{\min}\big) \quad \text{for } d_2 < x < d_3,\ t > 0,
\end{aligned}$$

where D_{NO} is the NO diffusion coefficient, k_1 is the rate constant of linear NO decay, $v_{\max}^{\mathrm{NO}}$ is the maximal rate of nonlinear NO decay, k_M^{NO} is the MM constant for nonlinear NO decay, and $Ca^{\min}$ is the minimal (background) Ca^{2+} concentration maintained in the postsynaptic terminal.

The conjugation conditions at $x = d_2$ and the zero-flux boundary conditions for $x = 0$ and $x = d_3$ are defined.

The Glu concentration in the synaptic cleft is determined by the equation

$$\frac{\partial[Glu]}{\partial t} = D_{\mathrm{Glu}}\frac{\partial^2[Glu]}{\partial x^2} - k_4[Glu] \quad \text{for } d_1 < x < d_2,\ t > 0,$$

with the Glu diffusion coefficient D_{Glu} and the effective rate constant of Glu decay k_4.

The Glu release into the synaptic cleft is triggered by the presynaptic action potential. To model the synaptic release of Glu, we use the time-dependent piece-wise constant function

$$\phi(t) = \begin{cases} 1, & t_{\mathrm{APstart}} \leqslant t \leqslant t_{\mathrm{APend}}, \\ 0 & \text{otherwise}, \end{cases}$$

where t_{APstart} and t_{APend} are the start and end time moments of the presynaptic action potential. The Glu release to the synaptic cleft from the presynaptic terminal is modeled as NO-independent and NO-dependent processes. The synaptic release of Glu during an action is described by the boundary condition

$$[Glu] = J_{\mathrm{Glu}}\left(1 + \frac{v_{\max}^{\mathrm{Glu}}}{k_M^{\mathrm{Glu}} + [NO]}[NO]\right)\phi(t) \quad \text{if } \phi(t) \neq 0 \text{ for } x = d_1,\ t > 0,$$

where J_{Glu} is the concentration of Glu during action potential at $x = d_1$ in the absence of NO, $v_{\max}^{\mathrm{Glu}}$ is the normalized maximal rate of NO-dependent Glu production, and k_M^{Glu} is the MM constant for NO-dependent Glu production.

The zero-flux boundary conditions at rest for $x = d_1$ and $x = d_2$ are defined.

The following equation characterizes the kinetics of Ca^{2+} in the postsynaptic neuron:

$$\frac{\partial [Ca]}{\partial t} = D_{\mathrm{Ca}} \frac{\partial^2 [Ca]}{\partial x^2} - k_5\big([Ca] - Ca^{\min}\big) \quad \text{for } d_2 < x < d_3,\ t > 0,$$

where D_{Ca} is the Ca^{2+} diffusion coefficient, and k_5 is the effective rate constant of Ca^{2+} decay. The Ca^{2+} enters postsynaptic terminal through the NMDA Glu receptors at Ca^{2+}. This is reflected in the boundary condition

$$D_{\mathrm{Ca}} \frac{\partial [Ca]}{\partial x} = -k_6\big(\overline{Ca} - [Ca]\big)[Glu] \quad \text{for } x = d_2,\ t > 0,$$

where the constant k_6 reflects the effective conductance of NMDA receptors, and $\overline{Ca}$ is the concentration of calcium in the synaptic cleft. The zero-flux boundary condition at $x = d_3$ is defined.

Unless otherwise indicated, the zero initial conditions for $[NO]$ and $[Glu]$ and the condition $[Ca](0, x) = Ca^{\min}$ are used.

The following parameters for MM interactions were used:

$$k_M^{\mathrm{NO}} = 10^{-4}\,\mu\mathrm{M}, \qquad v_{\max}^{\mathrm{NO}} = 3 \cdot 10^{-7}\,\mu\mathrm{M\,ms^{-1}},$$
$$k_M^{\mathrm{Glu}} = 5.6 \cdot 10^{-3}\,\mu\mathrm{M}, \qquad v_{\max}^{\mathrm{glu}} = 5.6.$$

A detailed description of the remaining parameters and numerical investigation used are presented in [11]. The time intervals between stimuli are subjects of investigation and are specified in Section 3.1.

3 Results

3.1 Interstimulus interval and bistable LTP model behavior

In LTP model proposed in [10], just the residue of a NO is noticeable before the following stimulus when test pulses are delivered every 5 s. Therefore the model behavior, involving positive feedback via retrograde NO signaling, is determined by the residue NO concentration before the next stimuli. This was used to evaluate the behavior of the model [11]. We set the initial NO concentration $[NO]_0$, then after 5 s, delivered the first and, after 10 s, the second stimulus pulses. The initial NO concentration $[NO]_0$ was varied from 0 nM with an increment of 0.05 nM, and the following model behavior was assessed: how the difference $\Delta[NO]$ of NO just before the second and first stimulus pulses ($[NO]_2$ and $[NO]_1$, respectively) depends on the $[NO]$ peak during the first pulse ($[NO]_\mathrm{p}$) (Fig. 2a in [11]). This dependence indicates how the change $\Delta[NO]$ of NO concentration between pulses depends on the NO concentration peak $[NO]_\mathrm{p}$ during the first stimulus pulse.

This approach of analysis of the dependence of $\Delta[NO]$ on the level of $[NO]_\mathrm{p}$ is compatible with the classical stability analysis. The number of stationary states represents the number of points where $\Delta[NO] = 0$, and the number of stable stationary points represents the number of stable model states. The introduced model stability analysis allowed us to achieve a bistable model behavior by modifying interactions between substances modeled [11].

The proposed bistable LTP model behavior [11] characterized by the plot in Fig. 2(b) (solid line) has three stationary points. Two of them are stable and reflect the two possible states of the model: the resting point at S_1^o and the higher $[NO]$ level and therefore enhanced synaptic transmission, "high-memory" point (herinafter the memory point) at S_3^o (Fig. 2(b), solid line). The unstable stationary point S_2^o represents a critical, or threshold, point (herinafter the threshold point): if $[NO]_\mathrm{p} < S_2^o$, then the system moves toward S_1^o, and if $[NO]_\mathrm{p} > S_2^o$, then the system moves toward S_3^o.

In this study, we investigated the behavior of the proposed LTP model with physiologically relevant interstimulus intervals. The background activity in a brain corresponds to range of frequency, rather than on the specific frequencies: the main power spectra components of electroencephalogram (EEG) recordings at rest are at frequencies < 20 Hz [28]. Single cell in vivo recordings from experimental animals revealed that spontaneous firing of neurons is highly irregular, and the average frequency depends on a cell type: 0.14 Hz in hippocampal CA1 and CA3 pyramidal cells of mice [19]), 1 Hz in L5 visual cortical pyramidal neurons of rats [18], and 4 Hz in pyramidal cells of rat prefrontal cortex [4]. First, we tested if a model exhibits a bistable behavior with shorter interstimulus intervals T. The decrease of T will lead to a net increase in NO production. Therefore, while decreasing the interstimulus interval 5 s n times, we reduced the strength of positive feedback by decreasing the model parameter J_Glu describing the amount of glutamate release after each stimulus pulse by n times also. We found that the dependence of $\Delta[NO]$ on the level of $[NO]_\mathrm{p}$ has three stationary points and therefore exhibits a bistable behavior for $T > 0.02$ s (Fig. 2(a)). For further investigation of dependence of model behavior on the interstimulus interval, we used $T = 1$ s, which corresponds to 1 Hz,

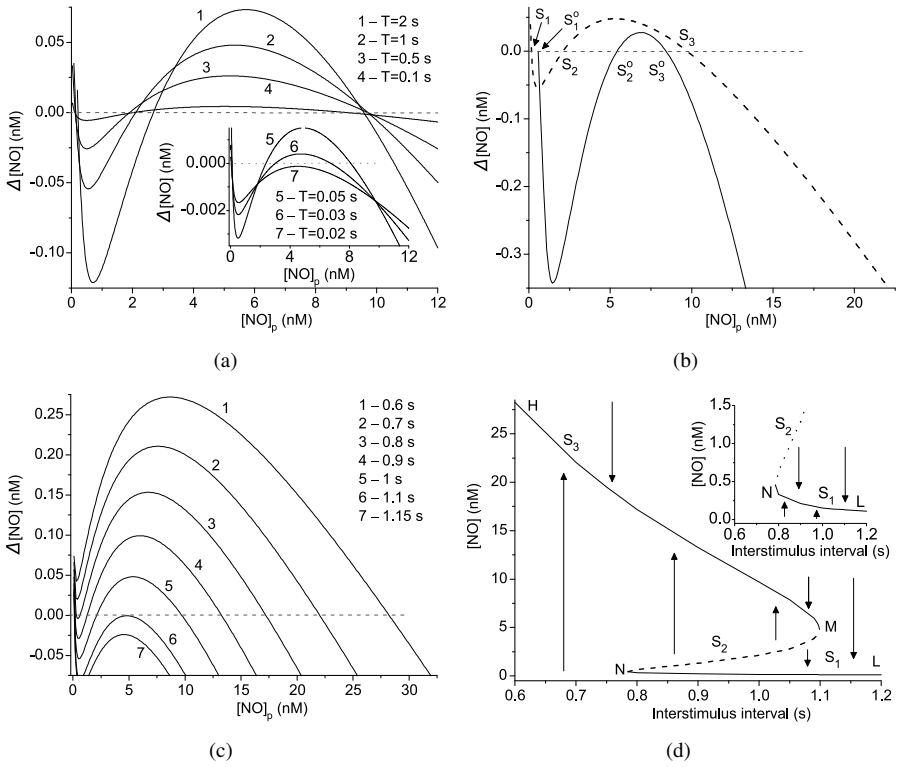

Figure 2. Influence of interstimulus interval on model behavior. (a) The influence of interstimulus interval on the dependence of $\Delta[NO]$ on the level of $[NO]_{\rm p}$. The values of $J_{\rm Glu}$ are 0.8 mM (1), 0.4 mM (2), 0.2 mM (3), 0.04 mM (4), 0.02 mM (5), 0.012 mM (6), and 0.008 mM (7). Insert presents a zoomed region of small $\Delta[NO]$ levels. (b) The dependence of $\Delta[NO]$ on the level of $[NO]_{\rm p}$ indicating the bistable behavior of model with three stationary points when interstimulus interval is 5 s ($J_{\rm Glu} = 2$ mM, solid line) and 1 s ($J_{\rm Glu} = 0.4$ mM, dashed line). (c) The influence of interstimulus interval T on the number of stationary points. (d) The dependence of stationary points on interstimulus interval. Insert presents a zoomed region of small $[NO]$ levels. Arrows indicate the direction of model evolution.

a frequency within a range of spontaneous firing recorded in vivo. The reduction of interstimulus interval and $J_{\rm Glu}$ resulted in bistable model behavior characterized by three new stationary points S_1, S_2, and S_3 (Fig. 2(b), dashed line).

The duration of interstimulus interval is a key parameter defining the balance between production and breakdown of NO. Therefore we investigated how the duration of interstimulus interval affects the dependence of $\Delta[NO]$ on the level of $[NO]_{\rm p}$ of model while other parameters are fixed (Fig. 2(c)). Reduction of interstimulus interval increases the value of memory point, decreases the value of threshold, and increases the value of resting point. This is summarized in Fig. 2(d), where dependence of resting, memory, and threshold points on interstimulus interval is displayed.

At certain interstimulus interval $T_N = 0.785$ s for a given model parameters, threshold and resting points fuse (saddle-node bifurcation point N in Fig. 2(d)), and at shorter

interstimulus intervals $T < T_N$, the threshold and resting points disappear (traces 1 and 2 in Fig. 2(c)), and there is just one stationary memory point. Similarly, when interstimulus interval exceeds $T_M = 1.1$ s, threshold and memory points fuse (saddle-node bifurcation point M in Fig. 2(d)), and at higher interstimulus intervals, the system has just one stationary resting point (trace 7 in Fig. 2(c)). Therefore the branch NL represents the resting points, MN the threshold points, and HM the memory points (Fig. 2(d)).

Model behavior changes qualitatively at saddle-node bifurcation points M and N (Fig. 2(d)). The LTP model for a range of interstimulus interval between T_N and T_M can be in one of two stable stationary states and therefore exhibits a bistable behavior.

The LTP model state (level of $[NO]$ and interstimulus interval) can be represented as a point in Fig. 2(d). If this point is on a branch LN or HM, then the LTP model is in a stationary resting or memory state, respectively. Changes in an activity of neuronal network will result in a change of interstimulus interval and therefore will result in horizontal shift of model state toward the corresponding value of new interstimulus interval T. Then the direction of model evolution toward the new steady stationary points depends on $[NO]$ level and is indicated by arrows in Fig. 2(d).

Figure 3(a) represents an example of model behavior when interstimulus interval is 1 s, which is between T_N and T_M. In this case the model exhibits the bistable behavior and, depending on initial $[NO]$ level ($[NO]_0$), evolves toward the resting point if $[NO]_0 < S_2$ (trace 1 in Fig. 3(a)) and toward the memory point if $[NO]_0 > S_2$ (traces 2 and 3 in Fig. 3(a)). When the interstimulus interval is 0.7 s, shorter than T_N (Fig. 3(b)), the model evolves toward the corresponding memory point for all values of $[NO]_0$ (traces 1–3 in Fig. 3(b)), and when interstimulus interval is 1.2 s, longer than T_M (Fig. 3(c)), the model evolves toward the corresponding resting point for all values of $[NO]_0$ (traces 1–3 in Fig. 3(c)).

These results indicate the importance of interstimulus intervals on modeled memory formation: the transition to "high-memory" state can be induced not only by a series of high-frequency (100 Hz) stimulation experimentally used for LTP induction, but also by a moderate decrease of interstimulus interval $T < T_N$. On the other hand, an increase of interstimulus $T > T_M$ would lead to "forgetting", moving of the model toward the resting point.

3.2 Model behavior during transient change of interstimulus interval

The interstimulus interval defines the number and values of stationary points and therefore the qualitative behavior of model. Moreover, due to balance between production and breakdown of NO, it also strongly influences the rate of evolution toward the stable stationary points. When the interstimulus interval $T > T_M$, the breakdown of NO dominates, the model evolves toward the resting point, and the rate of evolution increases with increase of interstimulus interval T (Fig. 4(a)). When the interstimulus interval $T < T_N$, production of NO dominates, and the rate of evolution toward memory point increases with decrease of interstimulus interval T (Fig. 4(b)). Therefore the duration of interstimulus interval T defines both the direction and rate of model evolution.

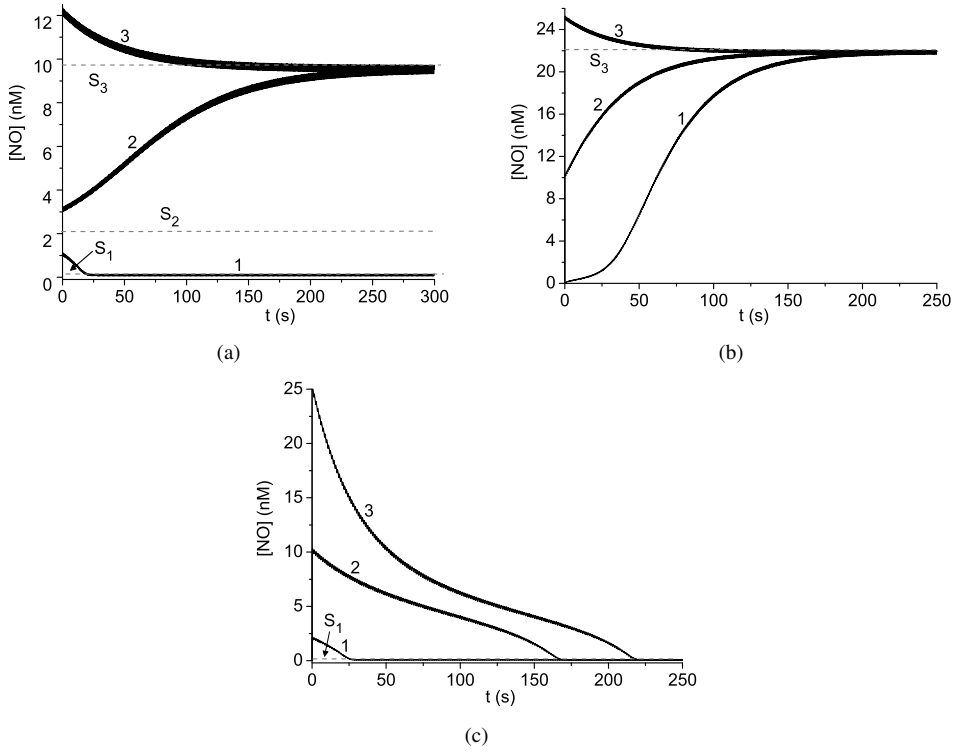

Figure 3. An example of model evolution from different initial levels of $[NO]_0$. (a) When interstimulus interval is 1 s, the model has three stationary points, two stable ones ($S_1 = 0.15$ nM and $S_3 = 9.7$ nM) and one unstable point ($S_2 = 2.12$ nM). Evolution of the model depends on the $[NO]_0$: if $[NO]_0 < S_2$, then the model evolves toward S_1 (trace 1); if $[NO]_0 > S_2$, then the model evolves toward S_3 (traces 2 and 3). (b) When the interstimulus interval is 0.7 s, then the model has just one stable stationary point $S_3 = 22$ nM and from all $[NO]_0$ evolves toward S_3. (c) When the interstimulus interval is 1.2 s, then the model has just one stable stationary point $S_1 = 0.12$ nM and from all $[NO]_0$ evolves toward S_1.

Changes in an activity of neuronal network will result in a transient change of interstimulus intervals and in a model evolution toward the new stationary state corresponding to the interstimulus interval.

For example, if at the memory state the interstimulus interval increases to from 1 s to 1.3 s, then at least 83 s are required for a level of $[NO]$ to cross the threshold S_2 at $T = 1$ s and "forgetting" the memory state (trace C in Fig. 4(c)). If the interstimulus interval increases to 2 s, then at least 31 s are required for "forgeting" the memory state (trace C in Fig. 4(d)). Decrease of interstimulus interval to a correspondingly shorter duration will result in model evolving back to the memory state (traces A and B in Figs. 4(c), 4(d)). Similarly, if at the resting state the interstimulus interval decreases from 1 s to 0.3 s, then to cross the threshold S_2 at $T = 1$ s or memory formation, it takes less than 4 s (trace C in Fig. 4(e)), and further model evolves toward the memory state. However, if the interstimulus interval decrease to 0.7 s, then at least 31 s are required for memory

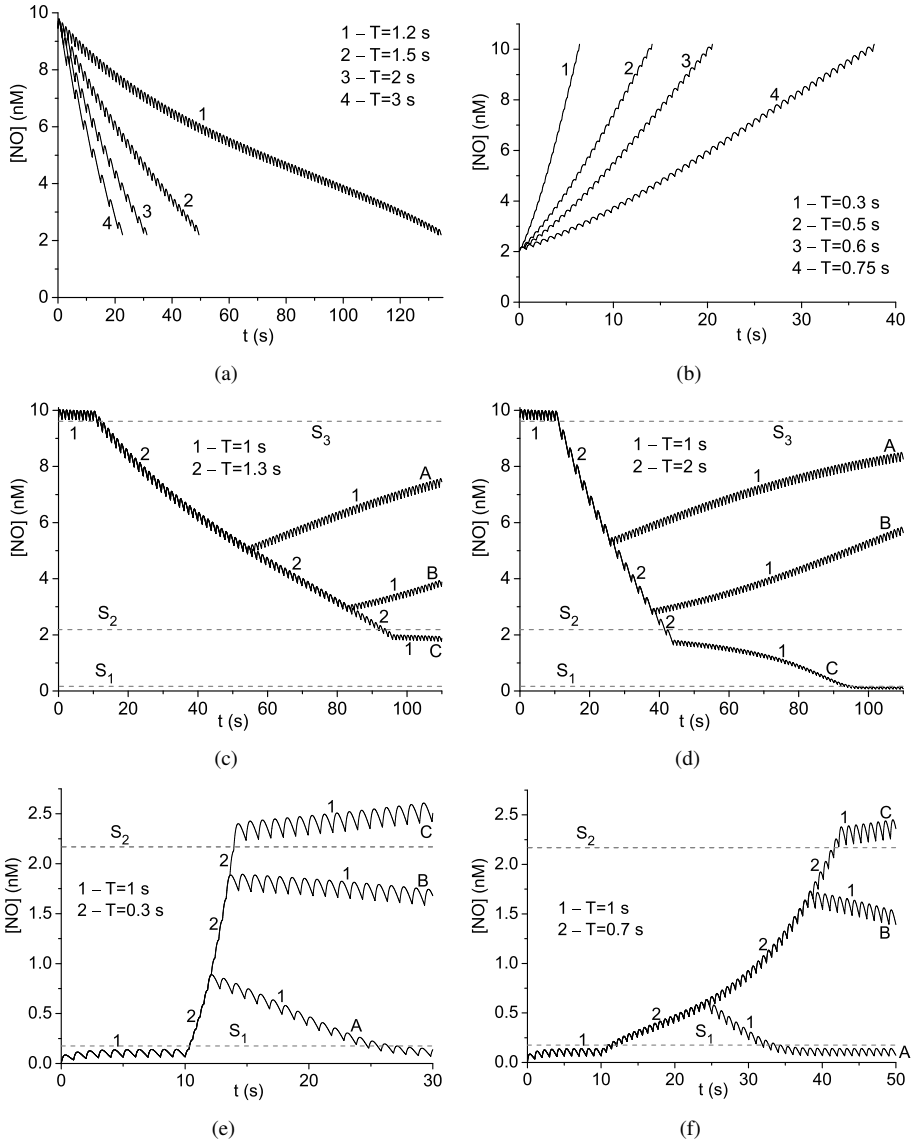

Figure 4. Model behavior during temporal change of interstimulus interval. The rate of NO decrease (a) and increase (b) depends on duration of interstimulus interval T. Temporal increase in interstimulus interval can lead to forgetting the memory state (traces C in (c), (d)), whereas temporal decrease in interstimulus interval can result in swithcing to the memory state (traces C in (e), (f)). The interstimulus intervals T are indicated in each panel.

formation (Fig. 4(f)). Increase of the interstimulus interval for a corresponding longer duration (traces A and B in Figs. 4(e), 4(f)) will result in model evolving back to the resting state.

These results indicate that both the level of transient change in neuronal activity (interstimulus interval T) and its duration determine whether the model ultimately changes its state.

3.3 Hysteresis-like model behavior

The dependence of LTP model stationary points on interstimulus interval has an inverted S-shape (Fig. 2(d)). This type of dependency, when in a range between T_N and T_M, the same interstimulus interval can correspond to two stable stationary states, imposes a hysteresis-like behavior. If the interstimulus interval decreases from higher values slowly (reaching the steady state at each point), the model remains in the resting state following the branch LN (Fig. 5(a)). At point N the model jumps toward the memory state

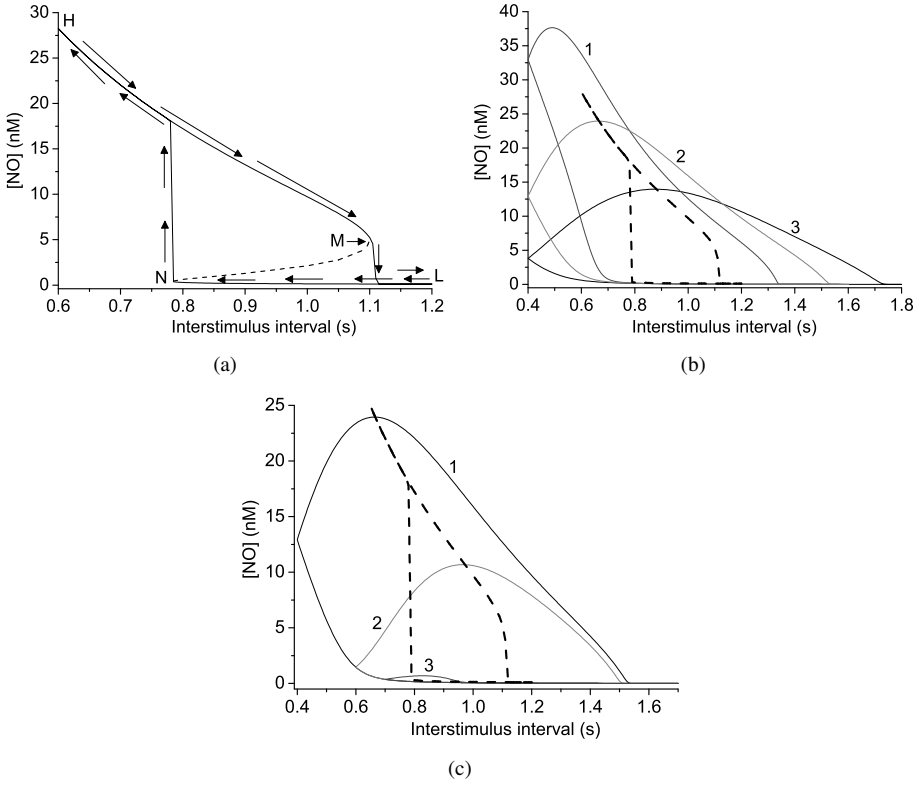

Figure 5. The hysteresis-like model behavior. (a) The hysteresis-like model behavior when the interstimulus interval T decreases slowly (reaching the steady state at each point) from 1.2 s to 0.6 s and then slowly increases back to 1.2 s. Arrows indicate the trajectory of model evolution. (b) The increase rate of change of interstimulus interval broadens the hysteresis. The increment/decrement of consecutive interstimulus intervals are 2 ms (1), 5 ms (2), 10 ms (3). (c) The decreased minimal interstimulus interval $T_{\min}$ broadens the hysteresis. $T_{\min}$: 0.4 s (1), 0.6 s (2), 0.7 s (3). An increment/decrement of consecutive interstimulus was 5 ms. Dashed lines in (b) and (c) represent the hysteresis-like trajectory from (a).

(branch MH, Fig. 5(a)) and evolves toward H. Then, if the interstimulus interval slowly increases, the model evolves following the branch HM in the memory state (Fig. 5(a)). At point M the model jumps toward the resting state (branch NL, Fig. 5(a)) and follows the branch NL. Therefore, between points N and M, the system can be in two stable (memory or resting) states. Moreover, the state depends on the history of model behavior.

During a pulse, just a limited amount of substances are released or produced. Moreover, the breakdown of NO takes time. Therefore some time is required for NO accumulation or breakdown (see Figs. 4(a), 4(b)). Figure 5(b) represents the hysteresis-like behavior of model when the interstimulus interval gradually decreases from 1.8 s to 0.4 s and then increases back to 1.8 s at different increments/decrements (the consequent intervals differ by 2 ms, 5 ms, and 10 ms). The increased rate of interstimulus interval change leads to broadening of hysteresis (Fig. 5(b)). Moreover, the transfer to resting states occurs at interstimulus intervals longer than T_M (Fig. 5(b)).

Moreover, the shape of hysteresis also depends on the value of minimal interstimulus interval ($T_{\min}$) reached during gradual decrease. If the interstimulus interval does not reach the T_N value, then system does not exhibit a hysteresis-like behavior. Hysteresis becomes noticeable when the interstimulus interval becomes smaller than T_N (trace 3 in Fig. 5(c)). Further decrease of interstimulus interval duration leads to broadening of hysteresis (traces 1 and 2 in Fig. 5(c)).

3.4 Parameter sensitivity of model behavior

The bistable behavior of the model is characterized by dependency of stationary points on interstimulus intervals (Fig. 2(c)), where branch LN correspond to the resting state, NM to the threshold point, and MH to the memory state. Here we tested how the dependency of stationary points on interstimulus intervals is affected by variation of parameters.

A detailed description of model parameters and their values used is provided in the methods section in [11]. The increase of model parameters by 20% had very little effect on the value of resting point for a given interstimulus interval (Fig. 6(a)). 20% increase in the MM constant for nonlinear NO decay (k_M^{NO}) and normalized maximal rate of NO-dependent Glu production ($v_{\max}^{\mathrm{Glu}}$) decreased the value of threshold (upward shift of NM, traces 2 and 5 in Fig. 6(a)), whereas 20% increase in maximal rate of nonlinear NO decay ($v_{\max}^{\mathrm{NO}}$) and the MM constant for NO-dependent Glu production (k_M^{Glu}) increased the value of threshold (downward shift of NM, traces 3 and 4 in Fig. 6(a)). 20% increase $v_{\max}^{\mathrm{Glu}}$ increased the value of memory state (upward shift of HM, trace 5 in Fig. 6(a)), whereas 20% increase in $v_{\max}^{\mathrm{NO}}$ and k_M^{Glu} decreased the value of memory state (downward shift of HM, traces 3 and 4 in Fig. 6(a)). 20% change in k_M^{NO} had little effect on the value of memory state (trace 2 in Fig. 6(a)).

Moreover, the change in model parameters affected the values of T_N and T_M of saddle-node bifurcation points M and N and therefore the interstimulus time range when the model exhibits a bistable behavior $[T_N, T_M]$ (Fig. 6). The points N and M were shifted to the right by 20% increase in k_M^{NO} and $v_{\max}^{\mathrm{Glu}}$ and to the left by 20% increase in $v_{\max}^{\mathrm{NO}}$ and k_M^{Glu} (Fig. 6(a)); however, the relative change of these parameters was less than

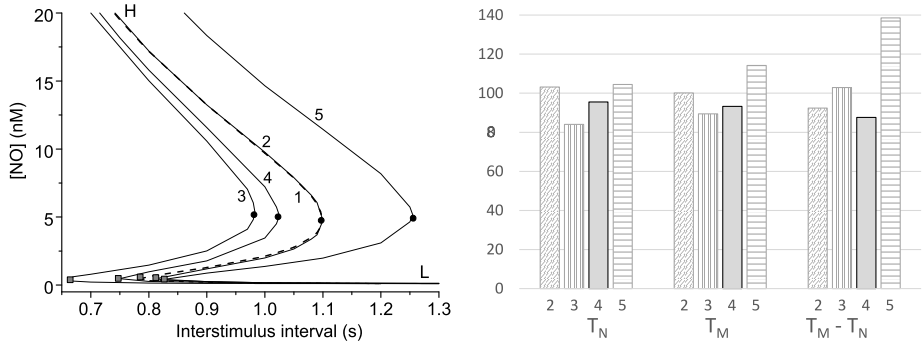

(a) (b)

Figure 6. Influence of model parameters on stationary states. (a) Influence of 20% increase of model parameter on the dependence of stationary points on interstimulus interval (• – the saddle-node bifurcation points M, □ – the saddle-node bifurcation points N). The plot from Fig. 2(d) (curve 1) and one parameter increased by 20%: $k_M^{\mathrm{NO}} = 1.2\cdot10^{-4}\ \mu\mathrm{M}$ (2), $v_{\max}^{\mathrm{NO}} = 3.6\cdot10^{-7}\ \mu\mathrm{M\,ms}^{-1}$ (3), $k_M^{\mathrm{Glu}} = 6.72\cdot10^{-3}\ \mu\mathrm{M}$ (4), $v_{\max}^{\mathrm{Glu}} = 6.72$ (5). (b) The relative value (%) of the T_N, T_M, and $T_M - T_N$ after 20% increase of the model parameter in (a).

20% (Fig. 6(b)). Parallel shift of N and M points resulted in shift rather than in change of the interstimulus interval range $[T_N, T_M]$ for bistable model behavior; however, 20% increase in $v_{\max}^{\mathrm{Glu}}$ parameter resulted in significant increased range of interstimulus interval for bistable model behavior by 40% (Fig. 6(b)).

The increase by 20% of tested model parameters affected the behavior of model. However, the effect was quantitative rather than qualitative. Therefore we conclude that the model behavior described is not limited to a specific set of model parameters.

4 Discussion

In this study, we investigated how the LTP model with positive feedback loop behaves in more physiological conditions when the changes in brain activity are reflected in changes of interstimulus intervals.

First, we demonstrated that interstimulus interval of 1 s, within a range of a typical background activity in a brain, is capable to maintain the level of NO sufficiently to keep the model in a high NO level or a memory state. Moreover, the moderate, less than 50%, and temporal decrease of the interstimulus interval is sufficient to trigger the transition of the system in to a high NO level state, or "memorizing". Even if the duration of interstimulus intervals returns to 1 s, the system can stay in a memory state for an infinite time. However, the moderate increase of interstimulus intervals leads to a transition toward the low $[NO]$ state or "forgetting". In this way the model under the physiological condition can be considered a bistable switch, where the output (strength of synaptic transmission) depends not just on instantaneous interstimulus intervals, but on the stimulus history as well. This means a hysteresis-like behavior with respect to changing duration of interstimulus interval.

These results provides a novel insight on the role of NO in synaptic transmission: positive feedback loop realized by NO can explain not just memory, but an advanced information processing as well.

Indeed, hysteresis-like model behavior can be deduced from the type of dependence of stationary points (resting point, memory point, and threshold point) on the interstimulus interval. For given model parameters, there are two saddle-node bifurcation points M and N. If the interstimulus interval decreases, then it will follow the resting state until the bifurcation point at T_M and the jump toward the memory. Further decrease of the interstimulus interval will result in model staying at the memory state. If being at the memory state, the interstimulus intervals starts to increase, then the model will stay in the memory state until the bifurcation point at T_N and then will jump to the resting state. Further increase of the interstimulus interval will result in the system following the "resting" trajectory. In this way, between saddle-node bifurcation points M and N, the model can be at two stable states, depending on the history of interstimulus intervals, and this will result in hysteresis-like model behavior.

A number of biological switches and oscillators exhibit a hysteresis-like behavior. This include circadian clock in mammals [1, 23], transitions of consciousness and unconsciousness in brain networks [12], gene regulatory networks [21, 32], calcium signaling [25, 29], water permeability switching in a synthetic membranes [8], and the cell cycle transition [6, 26]. The latter forms an irreversible hysteretic switch.

The hysteresis-like behavior is not advantageous for accurate control systems, as output depends not only on the instantaneous input, but on the input history as well. However, it enables systems to convert graded inputs into decisive, all-or-none outputs. Moreover, a hysteretic switching system with a wider safety zone can suppress the chattering, a phenomenon when a fluctuating system input is close to the transition threshold, and therefore can lead to too frequent switchings between the states. The hysteresis provides a "safety zone" against chattering over a wider range of stimuli and makes the system more resistant to noise [13].

The positive feedback loop in a synaptic transmission realized via retrograde signaling of NO exhibits a hysteresis like behavior. This extends functional features of model: it provides substrate not just for a memory formation, but also for reversible and weighted decision-making systems, where the decision depends not just on an instantaneous input, but on the history of input as well. The generation of action potentials in a brain is of stochastic nature [16, 30], and therefore a hysteresis-like behavior may assist in making a proper stable decision. Moreover, we have found that faster change in interstimulus intervals results in a broadening of hysteresis and, at the same time, increase of "safety zone" against chattering.

The single positive feedback loop via NO retrograde signaling is included in our model. Indeed, it is shown that the hysteretic switch can be implemented by a single positive feedback loop with a sufficiently large feedback strength [31]. However, the majority of biological systems exhibiting hysteresis are composed of coupled positive feedback loops [5], which increases robustness to noise. Including extra feedback loops (for example, for Ca^{2+} homeostasis) may enhance the stability of behavior of our model.

In this study, we used the interstimulus interval $T = 1$ s within a range of spontaneous firing activity recorded in vivo. The introduced proportional change of T and J_{Glu} resulted in bistable model behavior for $T > 0.02$ s. Therefore the use of interstimulus interval other than $T = 1$ s (for $T > 0.02$ s) will lead to quantitative rather than qualitative differences in model behavior. Moreover, the behavior of model for synaptic plasticity remains to be tested with interstimulus intervals of stochastic manner.

In conclusion, a model of synaptic plasticity, describing the behavior of positive feedback loop realized by NO, exhibits a hysteresis-like behavior and can explain not just memory, but an advanced information processing as well.

References

1. N. Barkai, S. Leibler, Circadian clocks limited by noise, *Nature*, **403**:267–268, 2000, https://doi.org/10.1111/febs.16065.
2. M.Z. Bin Ibrahim, A. Benoy, S. Sajikumar, Long-term plasticity in the hippocampus: Maintaining within and 'tagging' between synapses, *FEBS J.*, **289**:2176–2201, 2022, https://doi.org/10.1111/febs.16065.
3. R.D. Blitzer, Long-term potentiation: Mechanisms of induction and maintenance, *Sci. STKE*, **2005**(309):tr26, 2005, https://doi.org/10.1126/stke.3092005tr26.
4. J.M. Fellous, M. Rudolph, A. Destexhe, T.J. Sejnowski, Synaptic background noise controls the input/output characteristics of single cells in an in vitro model of in vivo activity, *Neurosci.*, **122**(3):811–829, 2003, https://doi.org/10.1016/j.neuroscience.2003.08.027.
5. J.E. Ferrell, Feedback regulation of opposing enzymes generates robust, all-or-none bistable responses, *Curr. Biol.*, **18**:R244–R245, 2008, https://doi.org/10.1016/j.cub.2008.02.035.
6. Z. Han, L. Yang, W.R. MacLellan, J.N. Weiss, Z. Qu, Hysteresis and cell cycle transitions: How crucial is it?, *Biophys. J.*, **88**:1626–1634, 2005, https://doi.org/10.1529/biophysj.104.053066.
7. B.E. Herring, R.A. Nicoll, Long-term potentiation: From CaMKII to AMPA receptor trafficking, *Annu. Rev. Physiol.*, **78**:351–365, 2016, https://doi.org/10.1146/annurev-physiol-021014-071753.
8. C.Y. Hu, A. Achari, P. Rowe, H. Xiao, S. Suran, Z. Li, K. Huang, C. Chi, C.T. Cherian, V. Sreepal, P.D. Bentley, A. Pratt, N. Zhang, K.S. Novoselov, A. Michaelides, R.R. Nair, pH-dependent water permeability switching and its memory in MoS2 membranes, *Nature*, **616**: 719–723, 2023, https://doi.org/10.1038/s41586-023-05849-4.
9. F. Jiang, S.T. Bello, Q. Gao, Y. Lai, X. Li, L. He, Advances in the electrophysiological recordings of long-term potentiation, *Int. J. Mol. Sci.*, **24**:7134, 2023, https://doi.org/10.3390/ijms24087134.
10. P. Katauskis, F. Ivanauskas, A. Alaburda, The "memory" effect in a chain of biochemical reactions with a positive feedback is enhanced by substrate saturation described by Michaelis–Menten kinetics, *Bull. Math. Biol.*, **81**:919–935, 2019, https://doi.org/10.1007/s11538-018-00541-5.

11. P. Katauskis, F. Ivanauskas, A. Alaburda, Mathematical model of synaptic long-term potentiation as a bistability in a chain of biochemical reactions with a positive feedback, *Acta Biotheor.*, **71**:16, 2023, https://doi.org/10.1007/s10441-023-09466-6.
12. H. Kim, J.-Y. Moon, G.A. Mashour, U. Lee, Mechanisms of hysteresis in human brain networks during transitions of consciousness and unconsciousness: Theoretical principles and empirical evidence, *PLoS Comput. Biol.*, **14**:e1006424, 2018, https://doi.org/10.1371/journal.pcbi.1006424.
13. J.-R. Kim, K.-H. Cho, The regulatory circuits for hysteretic switching in cellular signal transduction pathways, *FEBS J.*, **279**:3329–3337, 2012, https://doi.org/10.1111/j.1742-4658.2012.08623.x.
14. V. Klingel, J. Kirch, T. Ullrich, S. Weirich, A. Jeltsch, N.E. Radde, Model-based robustness and bistability analysis for methylation-based, epigenetic memory systems, *FEBS J.*, **288**:5692–5707, 2021, https://doi.org/10.1111/febs.15838.
15. R.N.L. Lamptey, B. Chaulagain, R. Trivedi, A. Gothwal, B. Layek, J. Singh, A review of the common neurodegenerative disorders: current therapeutic approaches and the potential role of nanotherapeutics, *Int. J. Mol. Sci.*, **23**:1851, 2022, https://doi.org/10.3390/ijms23031851.
16. P.R. Mendonça, M. Vargas-Caballero, F. Erdélyi, G. Szabø, O. Paulsen, H.P.C. Robinson, Stochastic and deterministic dynamics of intrinsically irregular firing in cortical inhibitory interneurons, *eLife*, **5**:e16475, 2016, https://doi.org/10.7554/eLife.16475.
17. M. Mincheva, G. Craciun, Multigraph conditions for multistability, oscillations and pattern formation in biochemical reaction networks, *Proc. IEEE*, **96**:1281–1291, 2008, https://doi.org/10.1109/JPROC.2008.925474.
18. K. Nataraj, N. Le Roux, M. Nahmani, S. Lefort, G. Turrigiano, Visual deprivation suppresses L5 pyramidal neuron excitability by preventing the induction of intrinsic plasticity, *Neuron*, **68**:750–762, 2010, https://doi.org/10.1016/j.neuron.2010.09.033.
19. K. Okamoto, T. Ishikawa, R. Abe, D. Ishikawa, C. Kobayashi, M. Mizunuma, H. Norimoto, N. Matsuki, Y. Ikegaya, Ex vivo cultured neuronal networks emit in vivo-like spontaneous activity, *J. Physiol. Sci.*, **64**:421–431, 2014, https://doi.org/10.1007/s12576-014-0337-4.
20. L.J. Ontañón-García, I. Campos Cantón, J. Pena Ramirez, Dynamic behavior in a pair of Lorenz systems interacting via positive-negative coupling, *Chaos Solitons Fractals*, **145**:110808, 2021, https://doi.org/10.1016/j.chaos.2021.110808.
21. M. Pájaro, I. Otero-Muras, C. Vázquez, A.A. Alonso, Transient hysteresis and inherent stochasticity in gene regulatory networks, *Nat. Commun.*, **10**:4581, 2019, https://doi.org/10.1038/s41467-019-12344-w.
22. Y. Penn, M. Segal, E. Moses, Network synchronization in hippocampal neurons, *Proc. Natl. Acad. Sci.*, **113**:3341–3346, 2016, https://doi.org/10.1073/pnas.1515105113.
23. J.P. Pett, A. Korenčič, F. Wesener, A. Kramer, H. Herzel, Feedback loops of the mammalian circadian clock constitute repressilator, *PLoS Comput. Biol.*, **12**:e1005266, 2016, https://doi.org/10.1371/journal.pcbi.1005266.
24. D. Puzzo, O. Vitolo, F. Trinchese, J.P. Jacob, A. Palmeri, O. Arancio, Amyloid-beta peptide inhibits activation of the nitric oxide/cGMP/cAMP-responsive element-binding protein pathway during hippocampal synaptic plasticity, *J. Neurosci.*, **25**:6887–6897, 2005, https://doi.org/10.1523/JNEUROSCI.5291-04.2005.

25. K.-R. Qin, C. Xiang, Hysteresis modeling for calcium-mediated ciliary beat frequency in airway epithelial cells, *Math. Biosci.*, **229**:101–108, 2011, https://doi.org/10.1016/j.mbs.2010.11.004.

26. A.F. Serpico, C. Pisauro, D. Grieco, On the assembly of the mitotic spindle, bistability and hysteresis, *Cell. Mol. Life Sci.*, **80**:83, 2023, https://doi.org/10.1007/s00018-023-04727-6.

27. O.A. Shipton, J.R. Leitz, J. Dworzak, C.E.J. Acton, E.M. Tunbridge, F. Denk, H.N. Dawson, M.P. Vitek, R. Wade-Martins, O. Paulsen, M. Vargas-Caballero, Tau protein is required for amyloid beta-induced impairment of hippocampal long-term potentiation, *J. Neurosci.*, **31**:1688–1692, 2011, https://doi.org/10.1523/JNEUROSCI.2610-10.2011.

28. P. Tarailis, F.M. De Blasio, D. Simkute, I. Griskova-Bulanova, Data-driven EEG theta and alpha components are associated with subjective experience during resting state, *J. Pers. Med.*, **12**(6), 2022, https://doi.org/10.3390/jpm12060896.

29. J.J. Torres, P.H.G.M. Willems, H.J. Kappen, W.J.H. Koopman, Hysteresis and bistability in a realistic model for IP3-driven Ca2+ oscillations, *Europhys. Lett.*, **55**:746, 2001, https://doi.org/10.1209/epl/i2001-00477-3.

30. C. van Vreeswijk, H. Sompolinsky, Chaos in neuronal networks with balanced excitatory and inhibitory activity, *Science*, **274**:1724–1726, 1996, https://doi.org/10.1126/science.274.5293.1724.

31. W. Xiong, J.E. Ferrell, A positive-feedback-based bistable 'memory module' that governs a cell fate decision, *Nature*, **426**:460–465, 2003, https://doi.org/10.1038/nature02089.

32. Y. Zhang, W. Yang, Y. Kumagai, M. Loza, W. Zhang, S.-J. Park, K. Nakai, Multi-omics computational analysis unveils the involvement of AP-1 and CTCF in hysteresis of chromatin states during macrophage polarization, *Front. Immunol.*, **14**, 2023, https://doi.org/10.3389/fimmu.2023.1304778.